

LatticeNet: Fast Point Cloud Segmentation Using Permutohedral Lattices

Radu Alexandru Rosu

Peer Schütt

Jan Quenzel

Sven Behnke

Abstract—Deep convolutional neural networks (CNNs) have shown outstanding performance in the task of semantically segmenting images. However, applying the same methods on 3D data still poses challenges due to the heavy memory requirements and the lack of structured data. Here, we propose LatticeNet, a novel approach for 3D semantic segmentation, which takes as input raw point clouds. A PointNet describes the local geometry which we embed into a sparse permutohedral lattice. The lattice allows for fast convolutions while keeping a low memory footprint. Further, we introduce DeformSlice, a novel learned data-dependent interpolation for projecting lattice features back onto the point cloud. We present results of 3D segmentation on various datasets where our method achieves state-of-the-art performance.

I. INTRODUCTION

Environment understanding is a crucial ability for autonomous agents. Perceiving not only the geometrical structure of the scene but also distinguishing between different classes of objects therein enables tasks like manipulation and interaction that were previously not possible. Within this field, semantic segmentation of 2D images is a mature research area, showing success stories in dense per pixel categorization on images [1]–[3]. However, the task of semantically labelling 3D data is still an open area of research as it poses several challenges that need to be addressed.

First, 3D data is often represented in an unstructured manner unlike the grid-like structure of images. This raises difficulties for current approaches which assume a regular structure upon which convolutions are defined.

Second, the performance of current 3D networks is limited by their memory requirements. Storing 3D information in a dense structure is prohibitive for even high-end GPUs, clearly showing the need for a sparse structure.

Third, discretization issues caused by imposing a regular grid onto point clouds can negatively affect the network’s performance and interpolation is necessary to cope with quantization artifacts [4].

In this work, we propose LatticeNet, a novel approach for point cloud segmentation which alleviates the previously mentioned problems. Hence, our contributions are:

- a hybrid architecture which leverages the strength of PointNet to obtain low-level features and 3D convolutions to aggregate global context,
- a framework suitable for sparse data onto which all common CNN operators are defined,

This work has been supported by the German Federal Ministry of Education and Research (BMBF) in the project “Kompetenzzentrum: Aufbau des Deutschen Rettungsrobotik-Zentrums” (A-DRZ).

All authors are with the Autonomous Intelligent Systems Group, University of Bonn, Germany rosu@ais.uni-bonn.de

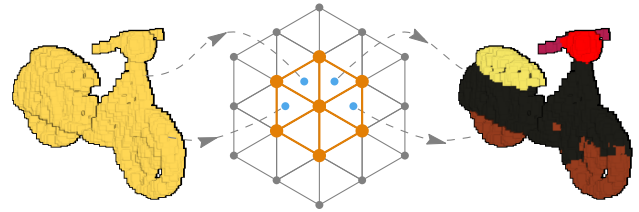


Fig. 1: Semantic segmentation: LatticeNet takes raw point clouds as input and embeds them into a sparse lattice where convolutions are applied. Features on the lattice are projected back onto the point cloud to yield a final segmentation.

- a novel slicing operator that is end-to-end trainable for mapping features of a regular lattice grid back onto an unstructured point cloud.

II. RELATED WORK

Semantic segmentation approaches applied to 3D data can be categorized depending on data representation upon which they operate.

Point cloud networks: The first category of networks operates directly on the raw point cloud.

From this area, PointNet [5] is one of the pioneering works. Their approach processes raw point clouds by individually embedding the points into a higher dimensional space and applying max-pooling for permutation-invariance to obtain a global scene descriptor. The descriptor can be used for both classification and semantic segmentation. However, PointNet does not take local information into account which is essential for the segmentation of highly-detailed objects. This has been partially solved in the subsequent work of PointNet++ [6] which applies PointNet hierarchically, capturing both local and global contextual information.

Chen et al. [7] use a similar approach but they input the points responses w.r.t. a sparse set of radial basis functions (RBF) scattered in 3D space. Optimizing jointly for the extent and center of the RBF kernels allows to obtain a more explicit modelling of the spatial distribution.

Instead, PointCNN [8] deals with the permutation invariance, not by using a symmetric aggregation function, but by learning a $K \times K$ matrix for the K input points that permutes the cloud into a canonical form.

Voxel networks: Voxel based approaches discretize the space in cubic or tetrahedral volume elements which are used for 3D convolutions.

SEGCloud [4] voxelizes the point cloud into a uniform 3D grid and apply 3D convolutions to obtain per-voxel class probabilities. A CRF is used to smooth the labels and enforce

global consistency. The class scores are transferred back to the points using trilinear interpolation. The usage of a dense grid results in high memory consumption while our approach uses a permutohedral lattice stored sparsely. Additionally, their voxelization results in a loss of information due to the discretization of the space. Our approach avoids quantization issues by using a PointNet architecture to summarize the local neighbourhood.

Rethage et al. [9] perform semantic segmentation on a voxelized point cloud and employ a PointNet architecture as a low level feature extractor. The usage of a dense grid, however, leads to high memory usage and slow inference, requiring various seconds for medium sized point clouds.

SplatNet [10] alleviates the computational burden of 3D convolutions by using a sparse permutohedral lattice, performing convolutions only around the surfaces. They discretize the space in uniform simplices and accumulate the features of the raw point cloud onto the vertices of the lattice using a splatting operation. Convolutions are applied on the lattice vertices and a slicing operation barycentrically interpolates the features of the vertices back onto the point cloud. A series of splat-conv-slice operations are applied to obtain contextual information. The main disadvantage is that splat and slice operations are not learned and repeated application slowly degrades the point clouds features as they act as Gaussian filters [11]. Furthermore, storing high dimensional features for each point in the cloud is memory intensive which limits the maximum number of points that can be processed. In contrast, our approach has learned operations for splatting and slicing which brings more representational power to the network and we also delegate their usage to only the beginning and the end of the network, leaving the rest of the architecture fully convolutional.

Mesh networks: Mesh based approaches operate on triangular or quadrilateral meshes. The connectivity information provided by the faces of the mesh allows to easily compute normal vectors and to establish local tangent planes.

GCNN [12] operates on small local patches which are convolved using a series of rotated filters followed by max pooling to deal with the ambiguity in the patch orientation. However, the max pooling disregards the orientation. MoNet [13] deals with the orientation ambiguity by aligning the kernels to the principal curvature of the surface. Yet, this doesn't solve cases in which the local curvature is not informative, e.g. for walls or ceilings. TextureNet [14] further improves on the idea by using a global 4-RoSy orientations field. This provides a smooth orientation field at any point on the surface which is aligned to the edges of the mesh and has only a 4 direction ambiguity. Defining convolution on patches oriented according to the 4-RoSy field yields significantly improved results.

Graph networks: Graph based approaches operate on vertices of a graph connected in an arbitrary topology, without the restrictions of triangular or quadrilateral meshes.

Wang et al. [15] and Wuet al. [16] define a convolution operator over non-grid structured data by having continuous values over the full vector space. The weights of these con-

tinuous filters are parametrized by an multi-layer perceptron (MLP).

Defferrard et al. [17] formulate CNNs in the context of spectral graph theory. They define the convolution in the Fourier domain with Chebychev polynomials to obtain fast localized filters. However, spectral approaches are not directly transferable to a new graph as the Fourier basis changes. Additionally, the learned filters are rotation invariant which can be seen as a limitation to the representational power of the network.

Multi-view networks: The convolution operation is well defined in 2D and hence, there is an interest in casting 3D segmentation as a series of multi view segmentations which are fused together.

Pham et al. [18] simultaneously reconstruct the scene geometry and recover the semantics by segmenting sequences of RGB-D frames. The segmentation is transferred from 2D images to the 3D world and fused with previous segmentations. A CRF finally resolves noisy predictions.

TangentConv [19] assumes that the data is sampled from locally Euclidean surfaces and project the local surface geometry onto a tangent plane to which 2D convolutions can be applied. A heavy preprocessing step for normal calculation is required. In contrast, our approach can deal with raw point clouds which are devoid of normal information.

III. NOTATION

Throughout this paper we use bold upper-case characters to denote matrices and bold lower-case characters to denote vectors.

The vertices of the d -dimensional permutohedral lattice are defined as a tuple $v = (\mathbf{c}_v, \mathbf{x}_v)$ with $\mathbf{c}_v \in \mathbb{Z}^{(d+1)}$ denoting the coordinates of the vertex and $\mathbf{x}_v \in \mathbb{R}^{v_d}$ representing the values stored at vertex v . The full lattice containing n vertices is denoted with $V = (\mathbf{C}, \mathbf{X})$ with $\mathbf{C} \in \mathbb{Z}^{n \times (d+1)}$ representing the coordinate matrix and $\mathbf{X} \in \mathbb{R}^{n \times v_d}$ the value matrix.

The points in a cloud are defined as a tuple $p = (\mathbf{g}_p, \mathbf{f}_p)$ with $\mathbf{g}_p \in \mathbb{R}^d$ denoting the coordinates of the point and $\mathbf{f}_p \in \mathbb{R}^{f_d}$ representing the features stored at point p (color, normals, etc). The full point cloud containing m points is denoted by $P = (\mathbf{G}, \mathbf{F})$ with $\mathbf{G} \in \mathbb{R}^{m \times d}$ being the positions matrix and $\mathbf{F} \in \mathbb{R}^{m \times f_d}$ the feature matrix. The feature matrix \mathbf{F} can also be empty in which case f_d is set to zero.

We denote with I_p the set of lattice vertices of the simplex that contains point p . The set I_p always contains $d+1$ vertices as the lattice tessellates the space in uniform simplices with $d+1$ vertices each. Furthermore, we denote with J_v the set of points p for which vertex v is one of the vertices of the containing simplices. Hence, these are the points that contribute to vertex v through the splat operation.

We denote with \mathcal{S} the splatting operation, with \mathcal{Y} the slicing operation, with $\tilde{\mathcal{Y}}$ the deformable slicing, with \mathcal{P} the PointNet module, with \mathcal{D}_G and \mathcal{D}_F the distribution of the point positions and the points features respectively and with \mathcal{G} the gathering operation.

IV. PERMUTOHEDRAL LATTICE

The d -dimensional permutohedral lattice is formed by projecting the scaled regular grid $(d+1)\mathbb{Z}^{d+1}$ along the vector $\mathbf{1} = [1, \dots, 1]$ onto the hyperplane $H_d: \mathbf{p} \cdot \mathbf{1} = 0$.

The lattice tessellates the space into uniform d -dimensional simplices. Hence, for $d = 2$ the space is tessellated with triangles and for $d = 3$ into tetrahedra. The enclosing simplex of any point can be found by a simple rounding algorithm [11].

Due to the scaling and projection of the regular grid, the coordinates \mathbf{c}_v of each lattice vertex sum up to zero. Each vertex has $2(d+1)$ immediate neighbouring vertices. The coordinates of these neighbours are separated by a vector of form $\pm[-1, \dots, -1, d, -1, \dots, -1] \in \mathbb{Z}^{d+1}$.

The vertices of the permutohedral lattice are stored in a sparse manner using a hash map in which the key is the coordinate \mathbf{c}_v and the value is \mathbf{x}_v . Hence, we only allocate the simplices that contain the 3D surface of interest. This sparse allocation allows for efficient implementation of all typical operations in CNNs (convolution, pooling, transposed convolution etc.).

The permutohedral lattice has several advantages w.r.t. standard cubic voxels. The number of vertices for each simplex is given by $d+1$ which scales linearly with increasing dimension, in contrast to the 2^d for standard voxels. This small number of vertices per simplex allows for fast splatting and slicing operations. Furthermore, splatting and slicing create piece-wise linear outputs as they use barycentric interpolation. In contrast, standard quantization in cubic voxels create piece-wise constant outputs, leading to discretization artefacts.

V. METHOD

The input to our method is a point cloud $P = (\mathbf{G}, \mathbf{F})$ containing coordinates and per-point features.

We define the scale of the lattice by scaling the positions \mathbf{G} as $\mathbf{G}_s = \mathbf{G}/\sigma$ where $\sigma \in \mathbb{R}^d$ is the scaling factor. The higher the sigma the less number of vertices will be needed to cover the point cloud and the coarser the lattice will be. For ease of notation, unless otherwise specified, we refer to \mathbf{G}_s as \mathbf{G} as we usually only need the scaled version.

A. Operations on Permutohedral Lattice

In this section we will explain in detail the standard operations on a permutohedral lattice that are used in previous works [10], [20].

Splatting refers to the interpolation of point features onto the values of the lattice V using barycentric weighting (Fig. 3a). Each point splats onto $d+1$ lattice vertices and their weighted features are summed onto the vertices.

Convoluting operates analogously to standard spatial convolutions in 2D or 3D, i.e. a weighted sum of the vertex values together with its neighbours. We use convolutions that span over the 1-hop ring around a vertex and hence convolve the values of $2(d+1)+1$ vertices (Fig. 2).

Slicing is the inverse operation to splatting. The vertex values of the lattice are interpolated back for each position

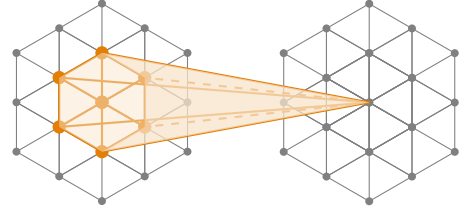


Fig. 2: Convolution: The neighbouring vertices of a lattice are convolved similarly to standard 2D convolutions. If a neighbour is not allocated in the sparse structure, we assume that it has a value of zero.

with the same weights used during splatting. The weighted contributions from the simplices $d+1$ vertices are summed up (Fig. 5a).

B. Proposed operations on Permutohedral Lattice

The operations defined in section Sec. V-A are typically used in a cascade of splat-conv-slice to obtain dense predictions [10]. However, splatting and slicing act as Gaussian kernel reducing encoded information [11]. Their repeated usage at every layer is detrimental to the accuracy of the network. Additionally, splatting acts as a weighted average on the feature vectors where the weights are only determined through barycentric interpolation. Including the weights as trainable parameter allows the network to decide on a better interpolation scheme. Furthermore, as the network grows deeper and feature vectors become higher dimensional, slicing consumes increasingly more memory, as it assigns the features to the points. Since in most cases $|P| \gg |V|$ it is more efficient to store the features only in the lattices vertices.

To solve these limitations, we propose four new operators on the permutohedral lattice which are more suitable for CNNs and dense prediction tasks.

Distribute is defined as the list of features that each lattice vertex receives. However, they are not summed as done by splatting:

$$\mathbf{x}_v = \mathcal{S}(P, V) = \sum_{p \in J_v} b_{pv} \mathbf{f}_p, \quad (1)$$

where \mathbf{x}_v is the value of lattice vertex v and b_{pv} is the barycentric weight between point p and lattice vertex v .

Instead, our distribute operators \mathcal{D}_G and \mathcal{D}_F concatenates coordinates and features of the contributing points:

$$\mathbf{x}_v = \mathcal{P}(\mathbf{D}_{v_g}; \mathbf{D}_{v_f}), \quad (2)$$

$$\mathbf{D}_{v_g} = \mathcal{D}_G(P, V) = \{ \mathbf{g}_p - \boldsymbol{\mu}_v \mid p \in J_v \}, \quad (3)$$

$$\mathbf{D}_{v_f} = \mathcal{D}_F(P, V) = \{ \mathbf{f}_p \mid p \in J_v \}, \quad (4)$$

$$\boldsymbol{\mu}_v = \frac{1}{|J_v|} \sum_{p \in J_v} \mathbf{g}_p. \quad (5)$$

where $\mathbf{D}_{v_g} \in \mathbb{R}^{|J_v| \times d}$ and $\mathbf{D}_{v_f} \in \mathbb{R}^{|J_v| \times f_d}$ are matrices containing the distributed coordinates and features respectively for the contributing points into a vertex v . The matrices are concatenated and processed by a PointNet \mathcal{P} to obtain

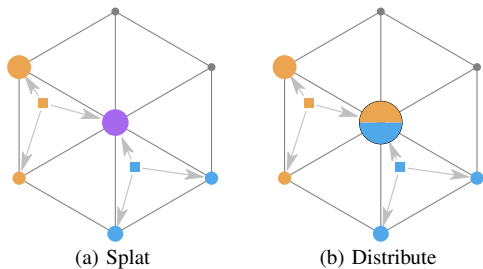


Fig. 3: Splat and Distribute operations: Splating uses barycentric weighting to add the features of points onto neighbouring vertices. The naïve summation can be detrimental to the network as splatting acts as a Gaussian filter. Distributing stores all the features of the contributing points, causing no loss of information and allows further processing by the network.

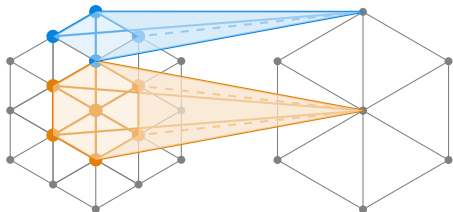


Fig. 4: Coarsen: Downsampling of the lattice is performed by embedding the coarse lattice in the finer one and convolving over the neighbours. This effectively performs a strided convolution. Transposed convolution is performed in an analogous manner by embedding a fine lattice into a coarse one.

the final vertex value x_v . Fig. 3 visualizes the difference between splatting and distributing.

Note that we use a different distribute functions for coordinates then for point features where we subtract the mean of the contributing coordinates. The intuition behind this is that coordinates by themselves are not very informative w.r.t. the potential semantic class. However, the local distribution is more informative as it gives a notion of the geometry.

Downsampling refers to a coarsening of the lattice, by reducing the number of vertices. This allows the network to capture more contextual information. Downsampling consists of two steps: creation of a coarse lattice and obtaining its values. Coarse lattices are created by repeatedly dividing the point positions by 2 and using them to create the vertices [21]. The values of the coarse lattice are obtained by convolving over the finer lattice from the previous level (Fig. 4). Hence, we must embed the coarse lattice inside the finer one by scaling the coarse vertices by 2. Afterwards, the neighbors vertices over which we convolve are separated by a vector of form $\pm [-1, \dots, -1, d, -1, \dots, -1] \in \mathbb{Z}^{d+1}$. The downsampling operation effectively performs a strided convolution.

Upsampling follows a similar reasoning. The fine vertices need first to be embedded in the coarse lattice using a division by 2. Afterwards the neighbouring vertices over which we convolve are separated by a vector of

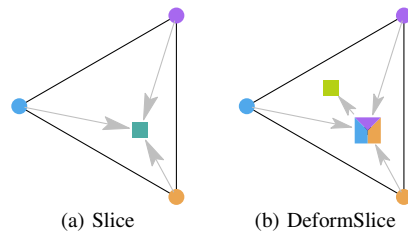


Fig. 5: Slice and DeformSlice: Slicing barycentrically interpolates the vertex values back onto a point. DeformSlice allows for the network to directly affect the interpolated value by learning offsets of the barycentric coordinates.

form $\pm [-0.5, \dots, -0.5, d/2, -0.5, \dots, -0.5]$. The upsampling operation effectively performs a transposed convolution.

DeformSlicing: While the slicing operation \mathcal{Y} barycentrically interpolates the values back to the points by using barycentric coordinates:

$$f_p = \mathcal{Y}(P, V) = \sum_{v \in I_p} b_{pv} x_v, \quad (6)$$

we propose the DeformSlicing $\tilde{\mathcal{Y}}$ which allows the network to directly modify the barycentric coordinates and shift the position within the simplex for data dependent interpolation:

$$f_p = \tilde{\mathcal{Y}}(P, V) = \sum_{v \in I_p} (b_{pv} + \Delta b_{pv}) x_v. \quad (7)$$

Here, Δb_{pv} are offsets that are applied to the original barycentric coordinates. A parallel branch within our network first gathers the values from all the vertices in a simplex and regresses the Δb_{pv} :

$$\mathbf{q}_p = \mathcal{G}(P, V) = \{ b_{pv} x_v \mid v \in I_p \}, \quad (8)$$

$$\Delta \mathbf{B} = \mathcal{F}(\mathbf{Q}). \quad (9)$$

The gathered values $\mathbf{q}_p \in \mathbb{R}^{(d+1)v_d}$ of the simplex containing p are combined for all points in the matrix $\mathbf{Q} \in \mathbb{R}^{m \times (d+1)v_d}$. The function \mathcal{F} defines the non-linear GN-ReLU-1x1 block which regresses the new barycentric coordinate offsets $\Delta \mathbf{B} \in \mathbb{R}^{m \times (d+1)}$. Barycentric coordinates by definition sum up to one, however the addition of the offset may break this assumption. We regularize the offsets to sum up to zero by adding an additional loss term:

$$L = \frac{1}{|P|} \sum_{p \in P} \left(\sum_{v \in I_p} \Delta b_{pv} \right)^2 \quad (10)$$

The difference between the slicing and our DeformSlicing is visualized in Fig. 5

VI. NETWORK

The input to our network is a point cloud P which may contain per point features stored in \mathbf{F} . The output is per-point class probabilities for each point p .

A. Architecture

Our network architecture has a U-Net structure [22] and is visualized in Fig. 6 together with the used individual blocks.

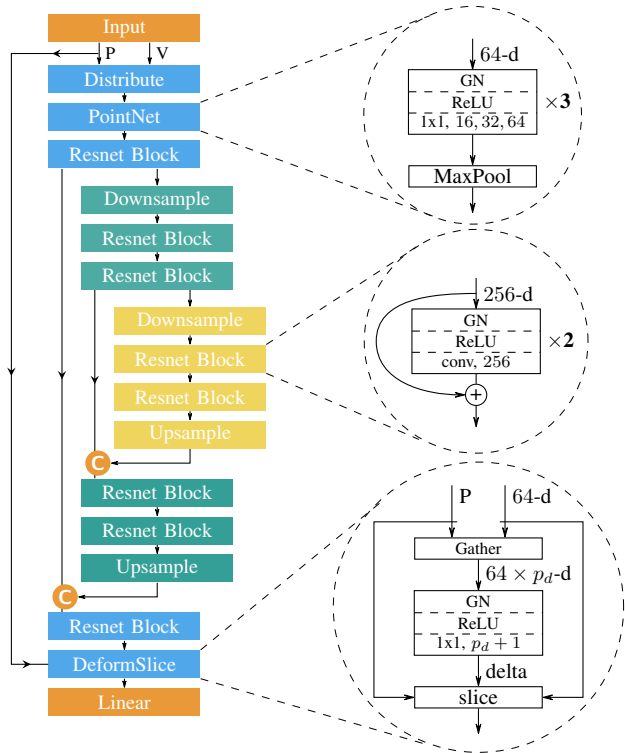


Fig. 6: Architecture: Our model follows a U-Net structure. For ease of representation, blocks which are repeated one after another are indicated with a multiplier on the right side of the operation.

The first layers distribute the point features onto the lattice and uses a PointNet to obtain local features. Afterwards a series of ResNet blocks [23] followed by repeated downsampling aggregates global context. The decoder branch mirrors the encoder architecture and upsamples through transposed convolutions. Finally a DeformSlicing propagates lattice features onto the original point cloud. Vertical connections are added by concatenating the encoder feature maps with matching decoder features.

All convolutions are pre-activated using Group Normalization [24] and a ReLU unit, following recent works [25], [26]. We choose Group Normalization instead of the standard batch normalization because it is more stable when the batch size is small.

VII. IMPLEMENTATION

Our lattice is stored sparsely on a hash map structure which allows for fast access of neighbouring vertices. Unlike [10], we construct the hash map directly on the GPU saving us from incurring an expensive CPU to GPU memory copy. All of the lattice operators containing forwards and backwards passes are implemented on the GPU and exposed to PyTorch [27]. Code and pretrained models will be made available upon acceptance.

The models were trained using the Adam optimizer, using a learning rate of 0.001 and a weight decay of 10^{-4} . The learning rate was reduced by a factor of 10 when the loss plateaued.

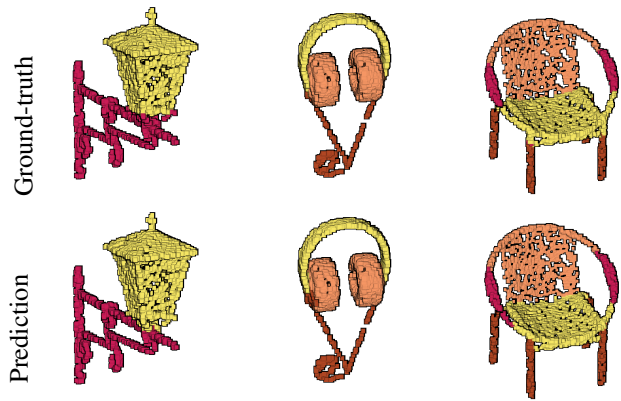


Fig. 7: ShapeNet [28] results

VIII. EXPERIMENTS

We evaluate our proposed lattice network on three different datasets on the task of semantic segmentation and report the mean Intersection over Union (mIoU). We use a shallow model for ShapeNet and a deeper model for ScanNet and SemanticKITTI as the datasets are larger. We augment all data using random mirroring and translations in space.

A. Datasets

ShapeNet part segmentation is a subset of the ShapeNet dataset [28] which contains objects from 16 different categories each segmented into 2 to 6 parts. The dataset consists of points sampled from the surface of the objects, together with the ground truth label of the corresponding object part. The objects have an average of 2613 points. We train and evaluate our network on each object individually. The results are gathered in Tab. I and visualized in Fig. 7.

ScanNet 3D segmentation [29] consists of 3D reconstructions of real rooms. It contains ≈ 1500 rooms segmented into 20 classes (bed, furniture, wall, etc.). The rooms have between 9K and 537K points and on average 145K. We segment an entire room at once without cropping.

SemanticKITTI [30] contains semantically annotated scans from the KITTI dataset which consists of laser scans from real urban environments. The scans are annotated with a total of 19 classes and each scan contains between 82K and 129K points. We process each scan entirely without any cropping. The results are provided in Tab. II. Our LatticeNet outperforms all other methods and in case of the most similar SplatNet by more than a factor of two.

B. Performance

We report the time taken for a forward pass and the maximum memory used in our shallow and deep network on the three evaluated datasets. The performance was measured on a NVIDIA Titan X Pascal and the results are gathered in Tab. IV. An X indicates methods that fail to process the full cloud due to memory limitations.

TABLE I: Results on ShapeNet part segmentation [28].

#instances	2690	76	55	898	3758	69	787	392	1547	451	202	184	283	66	152	5271	
	instance avg.	air-plane	bag	cap	car	chair	ear-phone	guitar	knife	lamp	laptop	motor-bike	mug	pistol	rocket	skate-board	table
PointNet [5]	83.7	83.4	78.7	82.5	74.9	89.6	73.0	91.5	85.9	80.8	95.3	65.2	93.0	81.2	57.9	72.8	80.6
PointNet++ [6]	85.1	82.4	79.0	87.7	77.3	90.8	71.8	91.0	85.9	83.7	95.3	71.6	94.1	81.3	58.7	76.4	82.6
SplatNet 3D [10]	84.6	81.9	83.9	88.6	79.5	90.1	73.5	91.3	84.7	84.5	96.3	69.7	95.0	81.7	59.2	70.4	81.3
SplatNet 2D-3D [10]	85.4	83.2	84.3	89.1	80.3	90.7	75.5	92.1	87.1	83.9	96.3	75.6	95.8	83.8	64.0	75.5	81.8
FCPN [9]	84.0	84.0	82.8	86.4	88.3	83.3	73.6	93.4	87.4	77.4	97.7	81.4	95.8	87.7	68.4	83.6	73.4
Ours	83.9	82.3	84.8	79.1	81.0	86.9	71.0	91.9	89.4	84.7	96.6	76.8	95.8	86.0	70.5	79.3	87.0

TABLE II: Results on SemanticKITTI [30].

Approach	mIoU	road	sidewalk	parking	other-ground	building	car	truck	bicycle	motorcycle	other-vehicle	vegetation	trunk	terrain	person	bicyclist	motorcyclist	fence	pole	traffic sign
PointNet [5]	14.6	61.6	35.7	15.8	1.4	41.4	46.3	0.1	1.3	0.3	0.8	31.0	4.6	17.6	0.2	0.2	0.0	12.9	2.4	3.7
SplatNet [10]	18.4	64.6	39.1	0.4	0.0	58.3	58.2	0.0	0.0	0.0	0.0	71.1	9.9	19.3	0.0	0.0	0.0	23.1	5.6	0.0
PointNet++ [6]	20.1	72.0	41.8	18.7	5.6	62.3	53.7	0.9	1.9	0.2	0.2	46.5	13.8	30.0	0.9	1.0	0.0	16.9	6.0	8.9
SqueezeSegV2 [31]	39.7	88.6	67.6	45.8	17.7	73.7	81.8	13.4	18.5	17.9	14.0	71.8	35.8	60.2	20.1	25.1	3.9	41.1	20.2	36.3
TangentConv [19]	40.9	83.9	63.9	33.4	15.4	83.4	90.8	15.2	2.7	16.5	12.1	79.5	49.3	58.1	23.0	28.4	8.1	49.0	35.8	28.5
DarkNet21Seg [30]	47.4	91.4	74.0	57.0	26.4	81.9	85.4	18.6	26.2	26.5	15.6	77.6	48.4	63.6	31.8	33.6	4.0	52.3	36.0	50.0
DarkNet53Seg [30]	49.9	91.8	74.6	64.8	27.9	84.1	86.4	25.5	24.5	32.7	22.6	78.3	50.1	64.0	36.2	33.6	4.7	55.0	38.9	52.2
Ours	52.2	88.8	73.8	64.6	25.6	86.9	88.6	43.3	12.0	20.8	24.8	76.4	57.9	54.7	34.2	39.9	60.9	55.2	41.5	42.7

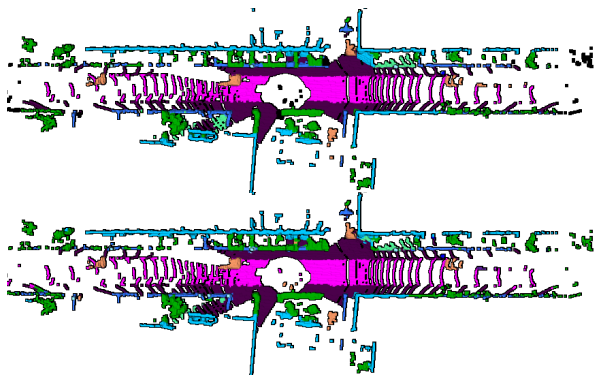


Fig. 8: SemanticKITTI results. The top image shows the ground truth and the bottom one our prediction.

TABLE III: Results on ScanNet [29]

Method	mIOU
PointNet++ [6]	33.9
SplatNet [10]	39.3
TangentConv [19]	43.8
3DMV [‡] [32]	48.4
MinkowskiNet42 (5cm) [33]	67.9
SparseConvNet [34] [†]	72.5
MinkowskiNet42 (2cm) [33] [†]	73.4
Ours	64.0

[†]: post-CVPR submissions. [‡]: uses 2D images additionally.

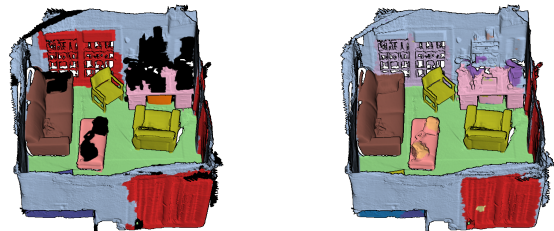


Fig. 9: ScanNet results. The left image shows the ground truth and the right one our prediction.

TABLE IV: Average time used by the forward pass and the maximum memory used during training.

	ShapeNet		ScanNet		SemanticKitti	
	[ms]	[GB]	[ms]	[GB]	[ms]	[GB]
SplatNet	129	0.6	X	X	2931	8.9
Ours	57	0.6	218	7.6	180	5.9

IX. CONCLUSION

We have presented LatticeNet, a novel method for semantic segmentation of points clouds. A sparse permutohedral lattice allows us to efficiently process large point clouds. The usage of PointNet together with a data-dependent interpolation alleviates the quantization issues of other methods. Experiments on three datasets show state of the art results, at a reduced time and memory budget. In the future we would like to incorporate temporal information into our model in order to process sequential data.

REFERENCES

- [1] J. Long, E. Shelhamer, and T. Darrell, "Fully convolutional networks for semantic segmentation," in *Proceedings of the IEEE conference on computer vision and pattern recognition*, 2015, pp. 3431–3440.
- [2] L.-C. Chen, G. Papandreou, F. Schroff, and H. Adam, "Rethinking atrous convolution for semantic image segmentation," *arXiv preprint arXiv:1706.05587*, 2017.
- [3] G. Lin, A. Milan, C. Shen, and I. Reid, "Refinenet: Multi-path refinement networks for high-resolution semantic segmentation," in *Proceedings of the IEEE conference on computer vision and pattern recognition*, 2017, pp. 1925–1934.
- [4] L. Tchapmi, C. Choy, I. Armeni, J. Gwak, and S. Savarese, "SEG-Cloud: Semantic segmentation of 3D point clouds," in *Proc. of the Intl. Conf. on 3D Vision (3DV)*. IEEE, 2017, pp. 537–547.
- [5] C. R. Qi, H. Su, K. Mo, and L. J. Guibas, "PointNet: Deep learning on point sets for 3D classification and segmentation," in *Proc. of the IEEE Conference on Computer Vision and Pattern Recognition (CVPR)*, 2017, pp. 652–660.
- [6] C. R. Qi, L. Yi, H. Su, and L. J. Guibas, "PointNet++: Deep hierarchical feature learning on point sets in a metric space," in *Advances in neural information processing systems*, 2017, pp. 5099–5108.
- [7] W. Chen, X. Han, G. Li, C. Chen, J. Xing, Y. Zhao, and H. Li, "Deep RBFNet: Point cloud feature learning using radial basis functions," *arXiv preprint arXiv:1812.04302*, 2018.
- [8] Y. Li, R. Bu, M. Sun, W. Wu, X. Di, and B. Chen, "PointCNN: Convolution on x-transformed points," in *Advances in Neural Information Processing Systems*, 2018, pp. 820–830.
- [9] D. Rethage, J. Wald, J. Sturm, N. Navab, and F. Tombari, "Fully-convolutional point networks for large-scale point clouds," in *Proc. of the European Conference on Computer Vision (ECCV)*, 2018, pp. 596–611.
- [10] H. Su, V. Jampani, D. Sun, S. Maji, E. Kalogerakis, M.-H. Yang, and J. Kautz, "SplatNet: Sparse lattice networks for point cloud processing," in *Proc. of the IEEE Conference on Computer Vision and Pattern Recognition (CVPR)*, 2018, pp. 2530–2539.
- [11] J. Baek and A. Adams, "Some useful properties of the permutohedral lattice for gaussian filtering," *In other words*, vol. 10, no. 1, p. 0, 2009.
- [12] J. Masci, D. Boscaini, M. Bronstein, and P. Vnderghynst, "Geodesic convolutional neural networks on riemannian manifolds," in *Workshop Proc. of the IEEE Int. Conference on Computer Vision (ICCV Workshops)*, 2015, pp. 37–45.
- [13] F. Monti, D. Boscaini, J. Masci, E. Rodola, J. Svoboda, and M. M. Bronstein, "Geometric deep learning on graphs and manifolds using mixture model cnns," in *Proc. of the IEEE Conference on Computer Vision and Pattern Recognition (CVPR)*, 2017, pp. 5115–5124.
- [14] J. Huang, H. Zhang, L. Yi, T. Funkhouser, M. Nießner, and L. J. Guibas, "TextureNet: Consistent local parametrizations for learning from high-resolution signals on meshes," in *Proc. of the IEEE Conference on Computer Vision and Pattern Recognition (CVPR)*, 2019, pp. 4440–4449.
- [15] S. Wang, S. Suo, W.-C. Ma, A. Pokrovsky, and R. Urtasun, "Deep parametric continuous convolutional neural networks," in *Proc. of the IEEE Conference on Computer Vision and Pattern Recognition (CVPR)*, 2018, pp. 2589–2597.
- [16] W. Wu, Z. Qi, and L. Fuxin, "Pointconv: Deep convolutional networks on 3d point clouds," in *Proc. of the IEEE Conference on Computer Vision and Pattern Recognition (CVPR)*, 2019, pp. 9621–9630.
- [17] M. Defferrard, X. Bresson, and P. Vnderghynst, "Convolutional neural networks on graphs with fast localized spectral filtering," in *Advances in neural information processing systems*, 2016, pp. 3844–3852.
- [18] Q.-H. Pham, B.-S. Hua, T. Nguyen, and S.-K. Yeung, "Real-time progressive 3D semantic segmentation for indoor scenes," in *IEEE Winter Conference on Applications of Computer Vision (WACV)*. IEEE, 2019, pp. 1089–1098.
- [19] M. Tatarchenko, J. Park, V. Koltun, and Q.-Y. Zhou, "Tangent convolutions for dense prediction in 3D," in *Proc. of the IEEE Conference on Computer Vision and Pattern Recognition (CVPR)*, 2018, pp. 3887–3896.
- [20] X. Gu, Y. Wang, C. Wu, Y. J. Lee, and P. Wang, "HPLFlowNet: Hierarchical permutohedral lattice FlowNet for scene flow estimation on large-scale point clouds," in *Proc. of the IEEE Conference on Computer Vision and Pattern Recognition (CVPR)*, 2019, pp. 3254–3263.
- [21] J. T. Barron, A. Adams, S. YiChang, and C. Hernández, "Fast bilateral-space stereo for synthetic defocus supplemental material," in *Proc. of the IEEE Conference on Computer Vision and Pattern Recognition (CVPR)*, 2015, pp. 1–15.
- [22] O. Ronneberger, P. Fischer, and T. Brox, "U-net: Convolutional networks for biomedical image segmentation," in *International Conference on Medical image computing and computer-assisted intervention*. Springer, 2015, pp. 234–241.
- [23] K. He, X. Zhang, S. Ren, and J. Sun, "Deep residual learning for image recognition," in *Proceedings of the IEEE conference on computer vision and pattern recognition*, 2016, pp. 770–778.
- [24] Y. Wu and K. He, "Group normalization," in *Proceedings of the European Conference on Computer Vision (ECCV)*, 2018, pp. 3–19.
- [25] K. He, X. Zhang, S. Ren, and J. Sun, "Identity mappings in deep residual networks," in *European conference on computer vision*. Springer, 2016, pp. 630–645.
- [26] G. Huang, Z. Liu, L. Van Der Maaten, and K. Q. Weinberger, "Densely connected convolutional networks," in *Proceedings of the IEEE conference on computer vision and pattern recognition*, 2017, pp. 4700–4708.
- [27] A. Paszke, S. Gross, S. Chintala, G. Chanan, E. Yang, Z. DeVito, Z. Lin, A. Desmaison, L. Antiga, and A. Lerer, "Automatic differentiation in PyTorch," in *NIPS Autodiff Workshop*, 2017.
- [28] L. Yi, V. G. Kim, D. Ceylan, I. Shen, M. Yan, H. Su, C. Lu, Q. Huang, A. Sheffer, L. Guibas, et al., "A scalable active framework for region annotation in 3D shape collections," *ACM Transactions on Graphics*, vol. 35, no. 6, p. 210, 2016.
- [29] A. Dai, A. X. Chang, M. Savva, M. Halber, T. Funkhouser, and M. Nießner, "ScanNet: Richly-annotated 3D reconstructions of indoor scenes," in *Proc. of the IEEE Conference on Computer Vision and Pattern Recognition (CVPR)*, 2017, pp. 5828–5839.
- [30] J. Behley, M. Garbade, A. Milioto, J. Quenzel, S. Behnke, C. Stachniss, and J. Gall, "SemanticKITTI: A dataset for semantic scene understanding of lidar sequences," in *Proc. of the IEEE Int. Conference on Computer Vision (ICCV)*, 2019.
- [31] B. Wu, X. Zhou, S. Zhao, X. Yue, and K. Keutzer, "Squeezesegv2: Improved model structure and unsupervised domain adaptation for road-object segmentation from a lidar point cloud," *arXiv preprint arXiv:1809.08495*, 2018.
- [32] A. Dai and M. Nießner, "3dmv: Joint 3d-multi-view prediction for 3d semantic scene segmentation," in *Proceedings of the European Conference on Computer Vision (ECCV)*, 2018, pp. 452–468.
- [33] C. Choy, J. Gwak, and S. Savarese, "4d spatio-temporal convnets: Minkowski convolutional neural networks," *arXiv preprint arXiv:1904.08755*, 2019.
- [34] B. Graham, M. Engelcke, and L. van der Maaten, "3d semantic segmentation with submanifold sparse convolutional networks," in *Proceedings of the IEEE Conference on Computer Vision and Pattern Recognition*, 2018, pp. 9224–9232.